ASN NEURO RESEARCH ARTICLE

ASN NEURO 4(1):art:e00072.doi:10.1042/AN20110038

Sensory neurons derived from diabetic rats have diminished internal Ca^{2+} stores linked to impaired re-uptake by the endoplasmic reticulum

Elena Zherebitskaya*, Jason Schapansky*,†, Eli Akude*,†, Darrell R Smith*,†, Randy Van der Ploeg*, Natasha Solovyova‡, Alexei Verkhratsky‡ and Paul Fernyhough*,†[1]

*Division of Neurodegenerative Disorders, St. Boniface Hospital Research Centre, Winnipeg, MB, Canada, R2H 2A6

†Department of Pharmacology and Therapeutics, University of Manitoba, Winnipeg, MB, Canada, R3E 0W3

‡Faculty of Life Sciences, University of Manchester, Manchester, U.K.

Cite this article as: Zherebitskaya E, Schapansky J, Akude E, Smith DR, Van der Ploeg R, Solovyova N, Verkhratsky A, Fernyhough P (2012) Sensory neurons derived from diabetic rats have diminished internal Ca^{2+} stores linked to impaired re-uptake by the endoplasmic reticulum. ASN NEURO 4(1):art:e00072.doi:10.1042/AN20110038

ABSTRACT

Distal symmetrical sensory neuropathy in diabetes involves the dying back of axons, and the pathology equates with axonal dystrophy generated under conditions of aberrant Ca^{2+} signalling. Previous work has described abnormalities in Ca^{2+} homoeostasis in sensory and dorsal horn neurons acutely isolated from diabetic rodents. We extended this work by testing the hypothesis that sensory neurons exposed to long-term Type 1 diabetes *in vivo* would exhibit abnormal axonal Ca^{2+} homoeostasis and focused on the role of SERCA (sarcoplasmic/endoplasmic reticulum Ca^{2+}-ATPase). DRG (dorsal root ganglia) sensory neurons from age-matched normal and 3–5-month-old STZ (streptozotocin)-diabetic rats (an experimental model of Type 1 diabetes) were cultured. At 1–2 days *in vitro* an array of parameters were measured to investigate Ca^{2+} homoeostasis including (i) axonal levels of intracellular Ca^{2+}, (ii) Ca^{2+} uptake by the ER (endoplasmic reticulum), (iii) assessment of Ca^{2+} signalling following a long-term thapsigargin-induced blockade of SERCA and (iv) determination of expression of ER mass and stress markers using immunocytochemistry and Western blotting. KCl- and caffeine-induced Ca^{2+} transients in axons were 2-fold lower in cultures of diabetic neurons compared with normal neurons indicative of reduced ER calcium loading. The rate of uptake of Ca^{2+} into the ER was reduced by 2-fold ($P<0.05$) in diabetic neurons, while markers for ER mass and ER stress were unchanged. Abnormalities in Ca^{2+} homoeostasis in diabetic neurons could be mimicked via long-term inhibition of SERCA in normal neurons. In summary, axons of neurons from diabetic rats exhibited aberrant Ca^{2+} homoeostasis possibly triggered by sub-optimal SERCA activity that could contribute to the distal axonopathy observed in diabetes.

Key words: axon plasticity, diabetic neuropathy, dorsal root ganglia (DRG), neurodegeneration, sarco/endoplasmic reticulum Ca^{2+}-ATPase (SERCA).

INTRODUCTION

Intracellular Ca^{2+} homoeostasis is, in part, regulated through activity of ER (endoplasmic reticulum) Ca^{2+} channels and Ca^{2+} binding proteins (Petersen et al., 2001; Verkhratsky and Petersen, 2002; Verkhratsky, 2005). Dynamic changes in free Ca^{2+} concentration within the ER and alterations in ER Ca^{2+} homoeostasis are critical regulators of cell function and survival (Mattson et al., 2001; Paschen and Frandsen, 2001; Glazner and Fernyhough, 2002, 2008; Verkhratsky and Petersen, 2002). The ER acts as a dynamic Ca^{2+} buffer as well as a primary store for intracellular Ca^{2+} signals, and ER Ca^{2+} release regulates neurotransmitter and hormone secretion, mitochondrial function, synaptic plasticity, expression of multiple genes and conveys Ca^{2+} signals from the cell periphery towards the nucleus (Verkhratsky and Toescu, 1998; Llano et al., 2000; Hardingham et al., 2001; Rose and Konnerth, 2001; Verkhratsky

[1]To whom correspondence should be addressed to (email paulfernyhough@yahoo.com).

Abbreviations: ATF3, activating transcription factor 3; AUC, area under the curve; $[Ca^{2+}]_I$, intracellular calcium concentration; $[Ca^{2+}]_{ER}$, ER calcium concentration; CaM, calmodulin; CCD, charge-coupled device; DRG, dorsal root ganglia; ER, endoplasmic reticulum; ERK, extracellular-signal-regulated kinase; Fura 2/AM, fura 2 acetoxymethyl ester; GRP78, glucose-regulated protein of 78 kDa; NT-3, neurotrophin-3; PBS-T, PBS with 0.05% Tween 20; PMPI, plasma membrane potential indicator; R123, rhodamine 123; RyR, ryanodine receptor; SERCA, sarco/ER Ca^{2+}-ATPase; SOCE, store-operated calcium entry; STIM, stromal interaction molecule; STZ, streptozotocin; TG, thapsigargin.

and Petersen, 2002; Verkhratsky, 2005). The ER Ca^{2+} homoeostasis and Ca^{2+} release are regulated by Ca^{2+} levels in the ER lumen (Burdakov et al., 2005), and therefore intra-ER Ca^{2+} levels represent a critical regulatory pathway for both cytoplasmic Ca^{2+} homoeostasis and mitochondrial function.

The handling of free Ca^{2+} within the cytosol and ER lumen is fundamentally different. Free $[Ca^{2+}]$ in the ER lumen ($[Ca^{2+}]_{ER}$ is ER calcium concentration) is three to four orders of magnitude greater than the cytosolic Ca^{2+} concentration ($[Ca^{2+}]_i$ is intracellular calcium concentration). This results in a steep concentration gradient and constant leakage of Ca^{2+} ions from the ER into the cytoplasm, which is counteracted by ER Ca^{2+} uptake driven by SERCA (sarco/endoplasmic reticulum calcium ATPase) pumps on the ER membrane. The ability of the ER to release Ca^{2+} in response to physiological stimulation is determined by three major types of channels: RyR (ryanodine receptor) and $InsP_3R$ (inositol triphosphate receptor) and receptors activated by NAADP (nicotinic acid–adenine dinucleotide phosphate) (Sitsapesan et al., 1995; Sutko and Airey, 1996; Patel et al., 2001; Thrower et al., 2001). Optimal $[Ca^{2+}]_i$ is maintained at ~100 nM by plasma membrane Ca^{2+}-ATPases and the SERCA pumps of the ER. Inhibition of ER Ca^{2+} uptake by blockade of SERCA or excessive Ca^{2+} release from ER by activation of ER-resident Ca^{2+} channels would alter this balance of Ca^{2+} such that $[Ca^{2+}]_{ER}$ would decrease and $[Ca^{2+}]_i$ would be elevated. Under high $[Ca^{2+}]_i$ the mitochondrion will increase Ca^{2+} uptake, leading to elevated $[Ca^{2+}]_m$ eventually resulting in organelle dysfunction. Depletion of $[Ca^{2+}]_{ER}$ is toxic to cells (Paschen and Frandsen, 2001; Patil and Walter, 2001) and may be more pathogenic even than elevated $[Ca^{2+}]_i$ (Verkhratsky, 2005).

Diabetic sensory neuropathy in humans is associated with structural changes in peripheral nerves, including segmental degeneration, microangiopathy, paranodal demyelination and loss of myelinated and unmyelinated fibres – the latter due to a dying-back of distal axons and characterized as reduced IENF (intra-epidermal nerve fibres) (Kennedy et al., 1996; Yagihashi, 1996; Malik et al., 2005; Quattrini et al., 2007; Ebenezer et al., 2011). Animal models of diabetic neuropathy reveal similar pathology and, in common with humans, exhibit sensory hypoalgesia and tactile allodynia (Christianson et al., 2003, 2007; Mizisin et al., 2007; Beiswenger et al., 2008; Jolivalt et al., 2008; Francis et al., 2009). The degenerative distal axonopathy observed in diabetes is also seen in cultured neurons isolated from diabetic rats (Zherebitskaya et al., 2009; Akude et al., 2010). We and others have demonstrated that experimental diabetes induces significant changes in Ca^{2+} homoeostasis in DRG (dorsal root ganglia) sensory neurons (Hall et al., 1995, 2001; Kostyuk et al., 1995, 2001; Voitenko et al., 1999, 2000; Huang et al., 2002, 2003; Kruglikov et al., 2004). This includes a steady-state increase in $[Ca^{2+}]_i$, increased high threshold Ca^{2+} currents and a decrease in the amplitude of depolarization-induced $[Ca^{2+}]_i$ signals. Most importantly, diabetes also leads to a significant decrease of caffeine-induced Ca^{2+} release from intracellular stores (Kostyuk et al., 2001; Huang et al., 2002; Kruglikov et al., 2004), suggesting altered ER Ca^{2+} homoeostasis. Therapy with low-dose insulin or NT-3 (neurotrophin-3) restored resting Ca^{2+} levels and depolarization- and caffeine-induced Ca^{2+} transients (Huang et al., 2002, 2003). Thus neurotrophic factor treatments which reverse diabetic neuropathic changes *in vivo* in STZ (streptozotocin)-diabetic rats may do so by restoring Ca^{2+} homoeostasis and/or mitochondrial function (Fernyhough et al., 2003; Huang et al., 2003, 2005a, 2005b). The purpose of the present study was to determine if axons, the primary site of neurodegeneration in diabetes, exhibit Ca^{2+} dyshomoeostasis and to focus on the role of a putative impairment in SERCA function as a key aetiological factor.

MATERIALS AND METHODS

Induction, treatment and confirmation of type 1 diabetes

Male Sprague–Dawley rats were made diabetic with a single intraperitoneal injection of 75 mg/kg STZ (Sigma). Starting body weights ranged from 275 to 325 g. At study end, body weights of age-matched controls were 717.8 ± 71.0 g and for STZ-induced diabetic rats weights were 428.1 ± 48.9 g (means $\pm$ S.D., $n=20$). All diabetic rats exhibited blood [glucose]>25 mM. At 3 months all animals were assessed for hind-paw thermal sensitivity using the Hargreaves apparatus, and diabetic cohorts exhibited significant signs of neuropathy, e.g. hypoalgesia (results not shown). Age-matched control or STZ-induced diabetic rats were maintained for 3–5 months, then were killed and DRG tissue collected for tissue culture. Animal procedures followed guidelines of University of Manitoba Animal Care Committee using Canadian Council of Animal Care rules.

Sensory neuron cultures and treatments

DRG from adult male Sprague–Dawley rats, age-matched control or STZ-induced diabetic (300–500 g), were dissociated using a previously described method (Huang et al., 2005b; Zherebitskaya et al., 2009). Neurons were cultured on to poly-DL-ornithine and laminin-coated 25 mm glass-bottomed dishes (Willco) in defined Hams F12 medium in the presence of modified Bottensteins N2 supplement without insulin (0.1 mg/ml transferrin, 20 nM progesterone, 100 μM putrescine, 30 nM sodium selenite and 1 mg/ml BSA; all additives were from Sigma; culture medium was from Life Technologies). The medium was also supplemented with a cocktail of sub-saturating neurotrophic factors [0.3 ng/ml NGF (nerve growth factor), 5 ng/ml GDNF (glial-derived neurotrophic factor) and 1 ng/ml NT-3]. In all studies, normal neurons were cultured in the presence of 10 mM glucose and 10 nM insulin. In all studies, diabetic neurons were exposed to 25 mM glucose and no insulin to attempt to mimic hyperglycaemic conditions found in STZ-diabetic rats, as previously described (Zherebitskaya et al., 2009).

Culture inserts

Neurons were plated on six-well plate inserts, which have PET [poly (ethylene terephthalate)] membrane with translucent optical properties and 8 μm pores with a density of 2×10^5 pores/cm^2. This insert makes culturing suitable for growing the cell body and axon compartments of neurons on different sites of the membrane and to then separately collect these compartments in lysates for Western blotting (Zheng et al., 2001). Neurons were cultured on inserts for 2 days in defined Hams F12 medium in the presence of modified Bottensteins N2 supplement without insulin as described above. The purity of axonal versus cell body samples was checked by immunostaining or Western blotting for the neuronal-specific nuclear protein ATF3 [activating transcription factor 3; antibody: ATF3 (C-19), 1:100, Santa Cruz]. Hanging cell culture inserts were purchased from Millipore.

Fluo-4/AM (acetoxymethyl ester)-based relative intracellular Ca^{2+} level analysis

Lumbar DRG neurons from age-matched control or 3–5 month STZ-induced diabetic rats were cultured for 1 day and then were loaded for 45 min at 37°C with 1 μM Fluo-4/AM (Invitrogen) to estimate relative intracellular Ca^{2+} levels in the axons. KCl (30 mM) and caffeine (20 mM) were added to the medium by perfusion for 10 s following baseline fluorescence measurements. Real-time imaging was done with a Carl Zeiss LSM510 confocal inverted microscope. Fluorescence was excited in single-track mode with the 488 nm band of the argon laser and emission detected with an LP 530 filter. High-resolution scanning was performed with a C-Aprochromat $63 \times /1.2$ w objective lens. The amplifier gain was kept constant throughout. All axons in each field were assessed as average of fluorescence pixel intensity per axon at each time point using the Carl Zeiss software package. The fluorescence intensity levels are presented relative to baseline and shown as $\Delta F/F$. Data were transferred into MS-Excel program for further statistical analysis.

Plasma membrane potential imaging

Plasma membrane potential was measured in cultured neurons using a PMPI (plasma membrane potential indicator; a proprietary component of the kit) from the Molecular Devices membrane potential assay kit. Dye was reconstituted in 1 ml of distilled water (PMPI stock) and was used at 1:3000 dilution. Cultured lumber DRG neurons were incubated with PMPI at 37°C for 1 h. KCl was added into the medium by perfusion for 10 s to a final concentration of 30 mM following baseline fluorescence measurements. Changes in fluorescence in axons were assessed with a Carl Zeiss LSM510 confocal inverted microscope as described above.

Mag-Fura patch-clamp

The intraluminal ER Ca^{2+} concentration was measured in neuronal cell bodies as described previously (Solovyova and Verkhratsky, 2002; Solovyova et al., 2002). Briefly, for ER ($[Ca^{2+}]_{ER}$) measurements cells were loaded with AM derivatives of Mag-Fura 2. The AM form of the indicator can passively diffuse across cell membranes. Once inside the cell, cytosolic and organelle esterases cleave the ester group off the probe, restoring the active Ca^{2+}-binding form of the indicator, and confining the indicator within different intracellular compartments. Loading at 37°C is favoured due to entrapment into intracellular organelles. In the patch-clamp configuration, the cytosolic dye was washed out into the pipette allowing selective imaging of the fluorescence of the dye trapped within the ER lumen. The Mag-Fura 2 was calibrated *in situ* using an ionomycin technique (see Solovyova et al., 2002). Fluorescence images were captured using an Olympus IX70 inverted microscope ($\times 40$ UV objective) equipped with a CCD (charge-coupled device) cooled intensified camera (Pentamax Gene IV; Roper Scientific). The specimen was alternately illuminated at 340, 380 and 488 nm by a monochromator (Polychrom IV; TILL Photonics) at a cycle frequency 3–5 Hz. Control over the experiment, image storage and off-line analysis was performed by use of MetaFluor/MetaMorph software (Universal Imaging Corporation) running on a Windows 98 workstation.

Fura 2/AM (fura 2 acetoxymethyl ester) ratiometric $[Ca^{2+}]_i$ determination and R123 (rhodamine 123) fluorescence imaging

DRG neurons were isolated from Sprague–Dawley rats and cultured on 35 mm glass-bottomed dishes. After 24 h in culture, neurons were treated with different doses of TG (thapsigargin; Sigma) for an additional 24 h prior to calcium imaging. Medium was then removed and cells were incubated in loading buffer (140 mM NaCl, 3 mM KCl, 2 mM $CaCl_2$, 2 mM $MgCl_2$, 10 mM glucose and 20 mM Hepes/NaOH, pH 7.4) with 5 μM Fura 2/AM for 30 min. Fura 2/AM was removed and cells washed three times in buffer, before adding fresh buffer containing 5 μM R123. After an additional 30 min, dishes were imaged on an Olympus IX70 Microscope connected to a CCD camera and perfusion system. Buffer was perfused over the cells at 2 ml/min to establish a baseline, prior to perfusing drugs over the cells for 30 s at the aforementioned flow rate. After calcium imaging, the perfusion system was deactivated and FCCP (carbonyl cyanide *p*-trifluoromethoxyphenylhydrazone; 10 μM) was added at the end of the experiment to assess mitochondrial inner membrane potential as previously described (Huang et al., 2002, 2005b). The R123 fluorescence intensity levels are presented relative to baseline and shown as $\Delta F/F$.

Immunocytochemistry for detection of calnexin and GRP78 (glucose-regulated protein of 78 kDa)

Cultures were fixed with 4% (w/v) paraformaldehyde in PBS (pH 7.4) for 15 min at room temperature (22°C) then permeabilized with 0.3% Triton X-100 in PBS for 5 min.

Cells were then incubated in blocking buffer (Roche) diluted with FBS and 1.0 mM PBS (1:1:3, by vol.) for 1 h then rinsed three times with PBS. Primary antibodies against calnexin (1:200; AbCam) and GRP78 BiP (1:400; AbCam) were used as ER stress markers and antibody to β-tubulin III (1:500; Sigma) was applied as a neuron marker and incubated at 4°C overnight. CY3- and FITC-conjugated secondary antibodies (1:250; Jackson ImmunoResearch Laboratories) were applied for 1 h at room temperature. All axons in each field were assessed as average of fluorescence pixel intensity for calnexin or GRP78 per axon at each time point. Axon length was derived from the β-tubulin III signal and expressed as mean pixel area. Cell body signals were deleted, and the fluorescence intensity signals for calnexin or GRP78 were expressed relative to the mean pixel area (β-tubulin III signal).

Western blotting for protein expression

Cultured DRG neurons were harvested after 48 h by scraping and lysates prepared in ice-cold stabilization buffer containing: 0.1 M Pipes, 5 mM $MgCl_2$, 5 mM EGTA, 0.5% Triton X-100, 20% glycerol, 10 mM NaF, 1 mM PMSF, and protease inhibitor cocktail (Fernyhough et al., 1999). Proteins were assayed using DC protein assay (Bio-Rad) and Western-blot analysis performed as previously described (Zherebitskaya et al., 2009). The samples (5 μg of total protein/lane) were resolved on an SDS/PAGE (10% gel) and electroblotted (100 V, 1 h) on to a nitrocellulose membrane. Blots were then blocked in 5% (w/v) non-fat dried skimmed milk powder containing 0.05% Tween overnight at 4°C, rinsed in PBS-T (PBS with 0.05% Tween 20) and then incubated with the primary antibody for calnexin (1:800; AbCam), GRP78 Bip (1:500; AbCam) and ATF3 (1:300; Santa Cruz). Total ERK (extracellular-signal-regulated kinase; 1: 2000; Santa Cruz Biotechnologies) was used as a loading control (previously demonstrated not to change under diabetic conditions). After four washes of 10 min in PBS-T, secondary antibody was applied for 1 h at room temperature. The blots were rinsed, incubated in Western Blotting Luminol Reagent (Santa Cruz Biotechnology), and imaged using the Bio-Rad Fluor-S image analyser.

Statistical analysis

Where appropriate, data were subjected to one-way ANOVA with *post-hoc* comparison using Dunnett's or Tukey's tests or regression analysis with a one-phase exponential decay parametric test with Fisher's parameter (GraphPad Prism 4, GraphPad Software Inc.). In all other cases two-tailed Student's *t* tests were performed.

RESULTS

Axons of sensory neurons derived from diabetic rats exhibit Ca^{2+} dyshomoeostasis

Lumbar DRG sensory neurons were isolated from age-matched control or 3–5-month-old STZ-induced diabetic rats and cultured simultaneously under defined conditions for 1–2 days. Neurons were loaded with Fluo-4/AM and then axonal fluorescence signals collected using a confocal microscope. Neurons were perfused for 10 s with either 30 mM KCl (Figure 1) or 20 mM caffeine (Figure 2) and relative alterations in $[Ca^{2+}]_i$ assessed in real time in axons. The KCl-induced depolarization-dependent rise in $[Ca^{2+}]_i$ peaked at approximately 4 s post-KCl

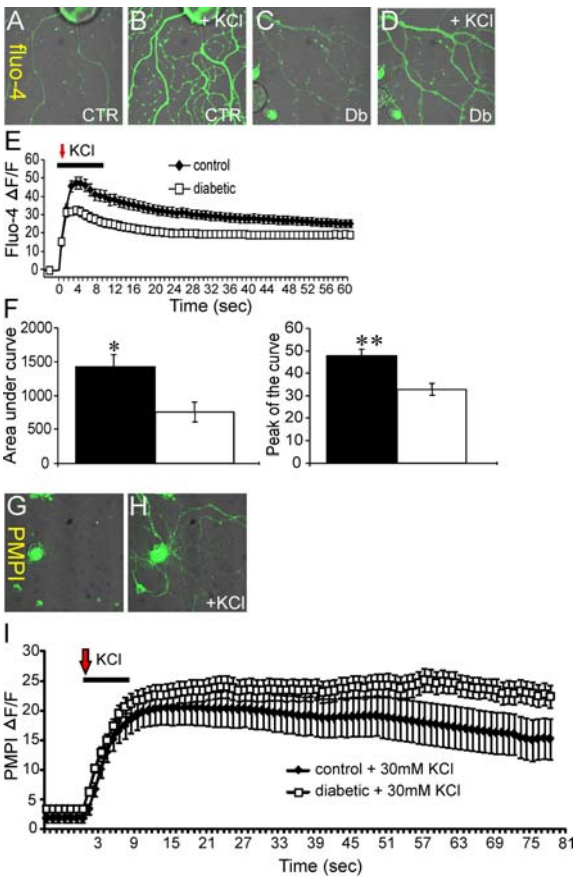

Figure 1 Axons of diabetic neurons exhibit impaired KCl-induced rise in intracellular Ca^{2+}

(**A–D**) Images of Fluo-4/AM fluorescence in the axons of cultured DRG neurons isolated from age-matched controls (CTR) or STZ-induced diabetic (Db) rats showing effect of 30 mM KCl (perfused for 10 s). The relative baseline Fluo-4/AM fluorescence intensity in axons was assessed for at least 1 min and was stable in all studies. In the traces shown the resting baseline Fluo-4/AM fluorescence intensity level has been arbitrarily set close to zero and change in fluorescence intensity shown as $\Delta F/F$. (**E**) Trace of Fluo-4/AM fluorescence signal in the axons of DRG neurons isolated from control (black diamonds) or diabetic (open squares) rats. The red arrow indicates point of injection of KCl. (**F**) AUC and peak of the curve for control (black bars) and diabetic (open bars). The Fluo-4/AM trace was characterized by non-linear regression (one phase exponential decay). The rate constant of decay (K)=0.03425±0.0008812 (control), 0.09634±0.005879 (diabetic). $t_{½}$ of decay=20 s (control) and 7 s (diabetic). The F (Fisher parameter) ratio=459, $P<0.0001$. The AUC was estimated from the baseline of normalized data (at the point of injection) to a fluorescence level of 0.4 and between time points of 3 s and 90 s using sums-of-squares. The peak of the curve was measured as highest value of the curve. The AUC and peak values are the means±S.E.M., n=78–91 axons; *$P<0.05$, **$P<0.001$, t test. In (**G**, **H**) are shown PMPI fluorescence signals. (**I**) Trace of PMPI fluorescence level after KCl injection. KCl affects plasma membrane potential at the same rate and value in axons of cultured sensory DRG neurons from control or diabetic rats.

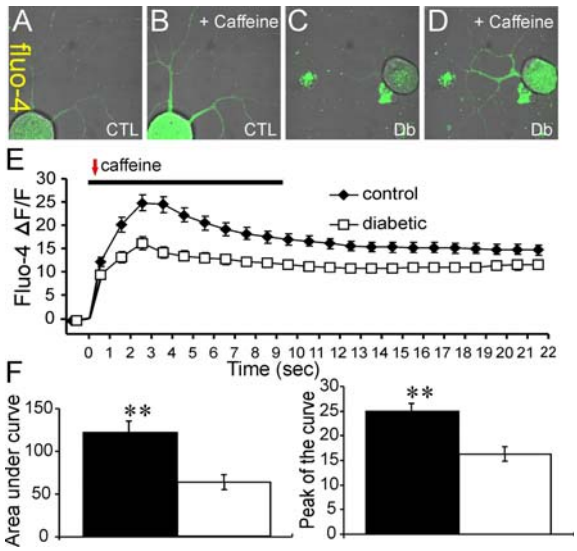

Figure 2 Axons of diabetic neurons exhibit impaired caffeine-induced Ca^{2+} release from the ER

(**A–D**) Images of Fluo-4/AM fluorescence in the axons of cultured DRG neurons isolated from age matched controls (CTL) and STZ-diabetic (Db) rats showing effect of 20 mM caffeine (perfused for 10 s). (**E**) Trace of Fluo-4/AM fluorescence signal in the axons of DRG neurons isolated from control (black diamonds) or diabetic (open squares) rats. The red arrow indicates point of injection of caffeine. (**F**) AUC and peak of the curve for control (black bars) and diabetic (open bars). The Fluo-4/AM trace was characterized by non-linear regression (one phase exponential decay). The rate constant of decay (K)=0.1086±0.01373 (control) and 0.07195±0.01678 (diabetic). $t_{½}$ of decay=6.4 s (control) and 9.6 s (diabetic). The F (Fisher parameter) ratio=22.8, $P<0.0001$. The AUC was estimated from the baseline of normalized data (at the point of injection) to a fluorescence level of 0.4 and between time points of 2 s and 22 s using sums-of-squares. The peak of the curve was measured as highest value of the curve. The AUC and peak values are the means±S.E.M., n=80–84 axons; $^{**}P<0.001$, t test.

treatment and regressed towards baseline by approximately 60 s (Figure 1E). The values for AUC (area under the curve) and peak amplitude were significantly lower in axons from diabetic neurons (Figure 1F). In Figures 1(G)–1(I), the PMPI signals are shown confirming that 30 mM KCl caused a significant depolarization of the neurons and that the degree of KCl-induced depolarization was similar for control and diabetic neurons. Caffeine-induced ER Ca^{2+} release was also quantified (Figure 2) and again in the axons of diabetic neurons the values for the AUC and peak amplitude for the rise in relative $[Ca^{2+}]_i$ were significantly lower. It is of note that, in response to KCl or caffeine, the transient change in $[Ca^{2+}]_i$ was not followed by a complete return to resting levels in axons of normal or diabetic neurons and may reflect impaired buffering capacity of Ca^{2+} in axons versus cell bodies.

Immunocytochemistry reveals reduced expression of calnexin in axons but no evidence of ER stress

The impaired Fluo-4/AM-based $[Ca^{2+}]_i$ responses in response to KCl and caffeine in axons could have been the result of loss of ER mass and/or induction of ER stress; therefore, neurons were stained for the ER marker, calnexin, and the ER stress indicator, GRP78. Neurons from control or diabetic rats were cultured for 1 day and exhibited specific and uniform antibody staining for calnexin across the cell body and axons of control and diabetic neurons (Figures 3A and 3B). The fluorescence intensity per axon for calnexin staining was determined and showed that, in diabetic neurons, there was a significant decrease in calnexin expression of 25% (Figure 3C). The antibody to GRP78 also gave specific and uniform staining and there was no difference in axonal staining intensity between control and diabetic cultures (Figures 3D–3F).

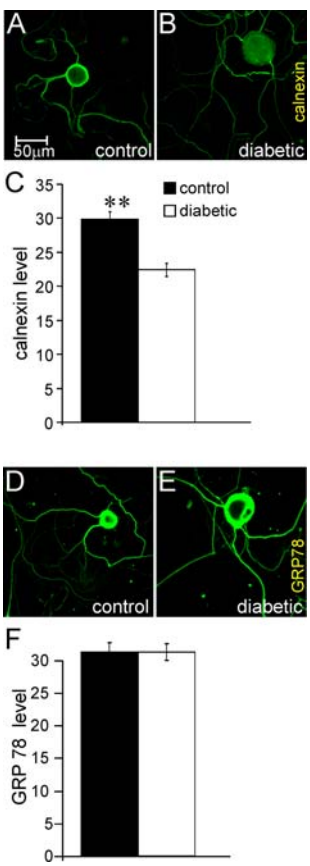

Figure 3 Immunocytochemistry of axons of cultured neurons from diabetic rats demonstrates a decrease in calnexin expression but no evidence of ER stress

(**A**, **B**) Representative immunofluorescent images of calnexin, (**D**, **E**) GRP78 protein levels in the axons of cultured DRG neurons (for 2 days) of age-matched controls or STZ-induced diabetic rats. These cultures were co-stained for neuron-specific β-tubulin III and the images shown are merged. (**C**, **F**) The quantification of calnexin and GRP78 proteins levels in axons respectively. Briefly, the fluorescence intensity signals for calnexin and GRP78 are expressed relative to the mean pixel area of the β-tubulin III signal, which provides a read-out of axon length (cell body signals were deleted from the calculation). Values are means±S.E.M., n=219–325 axons. $^{**}P<0.01$, t test.

Western blotting for expression of calnexin and GRP78 in axon versus cell body shows no effect of diabetes

We attempted to confirm the immunocytochemistry experiments using a Western blotting approach coupled with a culture system permitting separation of axon from cell body. Neurons were grown for 2 days on inserts with a mesh size allowing axons to grow through the mesh to the underside. Figures 4(A)–4(D) show immunostaining for neuron-specific β-tubulin III and the nuclear-specific ATF3 on the top versus underside of the culture inserts. The immunostaining demonstrates the underside of the membrane exhibited a purely axonal component. In Figure 4(E), Western blotting confirmed that ATF3 expression was restricted to the top surface corresponding with neuronal cell bodies. Neurons from age-matched control and STZ-induced diabetic rats were then grown on inserts for 2 days and the cell body versus axon tissue homogenates prepared and subjected to Western blotting (Figure 4F). Three independent experiments clearly demonstrated that expression of calnexin and GRP78 were similar between control and diabetic neurons in the cell body or axon compartments (Figure 4G).

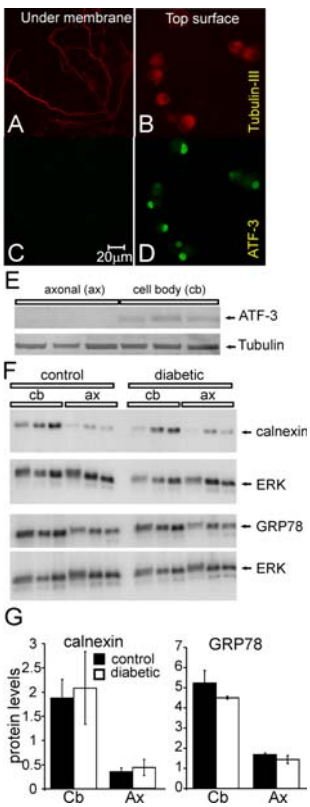

Figure 4 Western blotting of axonal versus cell body samples from culture inserts reveals no diabetes-induced change in expression of calnexin or GRP78

Cultures were grown up on insert membranes to enable separation of neuron cell bodies from axons. β-Tubulin III was used as a general neuron marker and ATF3 as a neuron cell body marker. (**A**, **B**) Typical immunofluorescent images of β-tubulin III showing staining of axons and cell bodies on both sides of membrane. Immunofluorescent images of ATF3 showing neuron cell body on the top surface (**D**), but not on the underside of the membrane (**C**). (**E**) Representative blots showing axon fraction purity. (**F**) Typical blots showing calnexin and GRP78 levels in the axons and cell body fractions in cultured DRG neurons isolated from age-matched controls or STZ-induced diabetic rats. (**G**) Quantification of calnexin and GRP78 protein levels in cell body and axon fractions from control (black bars) or diabetic (open bars) rats. Protein levels are presented relative to total ERK level. Values are means $\pm$ S.E.M. $n=3$ rats.

Ca^{2+} uptake into the ER is impaired in diabetic neurons

To test whether the deficiencies in $[Ca^{2+}]_i$ homoeostasis in diabetic neurons were due to reduced $[Ca^{2+}]_{ER}$, we compared intra-ER Ca^{2+} dynamics in normal and in diabetic neurons using direct recordings of $[Ca^{2+}]_{ER}$. Resting $[Ca^{2+}]_{ER}$ level was substantially reduced in cells from diabetic neurons (average values 244 ± 19 μM, $n=17$ for control neurons and 97 ± 21 μM, $n=7$ for diabetic neurons). To assess the rates of Ca^{2+} release, leakage and accumulation, we first stimulated the cells with caffeine (which induced RyRs opening and Ca^{2+} release from the ER; Figure 5A). After caffeine washout the $[Ca^{2+}]_{ER}$ returned to the pre-stimulated level because of SERCA-dependent Ca^{2+} uptake. Then the cells were stimulated with TG, which inhibited SERCA pumps and unmasked Ca^{2+} leakage from the ER that eventually led to the store depletion (Figure 5A). By plotting the rate of Ca^{2+} uptake/Ca^{2+} leakage

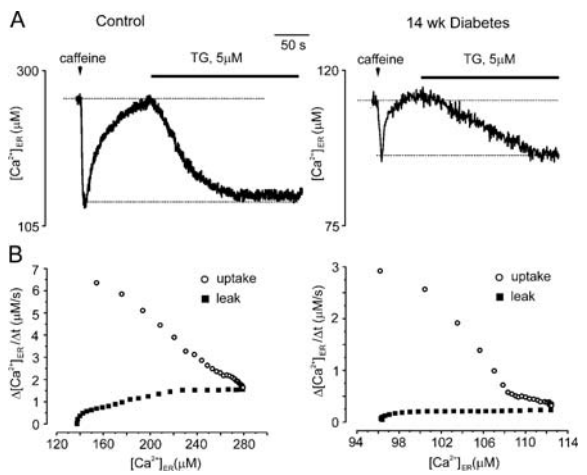

Figure 5 Rate of ER-dependent Ca^{2+} uptake is reduced in diabetic neurons

Sensory neurons were acutely isolated from control and 14-week-old STZ-diabetic rats, cultured for 2 h and then patched and ER Ca^{2+} was monitored using Mag-Fura 2 low affinity Ca^{2+}-sensitive fluorescent probes, as described previously (Solovyova et al., 2002). Values for resting $[Ca^{2+}]_{ER}$, Ca^{2+} release, re-uptake and Ca^{2+} leakage from the ER store in control and diabetic DRG neurons were defined. (**A**) Shows a representative $[Ca^{2+}]_{ER}$ trace and $[Ca^{2+}]_{ER}$ changes in control or 14-week-old diabetic neurons in response to 5 s application of 20 mM caffeine and application of 5 μM TG. The recovery of $[Ca^{2+}]_{ER}$ after washout of caffeine reflects the SERCA pump activity. The application of TG blocks SERCA pumps and therefore unmasks the resting Ca^{2+} leak from the ER lumen. (**B**) The first derivative of Ca^{2+} recovery and Ca^{2+} leakage are plotted against current $[Ca^{2+}]_{ER}$ for control and diabetic neurons. The maximal Ca^{2+} uptake rate in diabetic neurons is 2-fold smaller when compared with control neurons. A preliminary version of this work was presented by Verkhratsky and Fernyhough (2008).

versus actual $[Ca^{2+}]_{ER}$ (see Solovyova et al., 2002 for details), we found that both the maximal rate of Ca^{2+} reuptake and Ca^{2+} leakage were severely depressed in diabetic neurons (Figure 5B). On average the maximal Ca^{2+} re-uptake rate was 6 ± 0.85 μM/s, $n=6$ in control cells versus 2.7 ± 0.3 μM/s in diabetic neurons; the rates for maximal Ca^{2+} leakage were 1.5 ± 0.17 μM/s, $n=6$ and 0.37 ± 0.1 μM/s, $n=5$ for control and diabetic neurons respectively.

Long-term TG treatment of normal neurons induces Ca^{2+} dyshomoeostasis that mimics the diabetic state

Compromised Ca^{2+} accumulation into the ER could underlie aberrant Ca^{2+} homoeostasis in diabetes. This could be due to impaired activity and/or expression of SERCA and therefore, to further strengthen evidence for a role of SERCA in diabetes-induced abnormalities in sensory neuron phenotype, we exposed normal neurons for 1 day to different concentrations of TG, a specific and irreversible inhibitor of the SERCA pump, in order to artificially compromise SERCA function. Normal neurons were cultured for 1 day under defined conditions and in the presence of TG (3, 30 or 300 nM) and then loaded with Fura 2/AM to assess Ca^{2+} homoeostasis using ratiometric fluorescence imaging. Increasing TG from 3 to 300 nM caused a significant rise in the resting $[Ca^{2+}]_i$ in normal neurons (Figure 6B). Neurons were perfused for 30 s with 20 mM caffeine (Figure 6C) or 30 mM KCl (Figure 6D) and the maximum change in $[Ca^{2+}]_i$ is presented. Thapsigargin at 30 and 300 nM caused a significant decrease in the caffeine and KCl-induced rise in $[Ca^{2+}]_i$. In a separate study, normal neurons were treated for 1 day with 30 nM TG and then loaded simultaneously with Fura 2/AM and R123 for assessment of resting $[Ca^{2+}]_i$ and mitochondrial inner membrane potential. The resting $[Ca^{2+}]_i$ was again significantly raised from 148 to 320 nM in TG-treated cells and was paralleled with a depolarization of the mitochondrial inner membrane potential (Figure 6E).

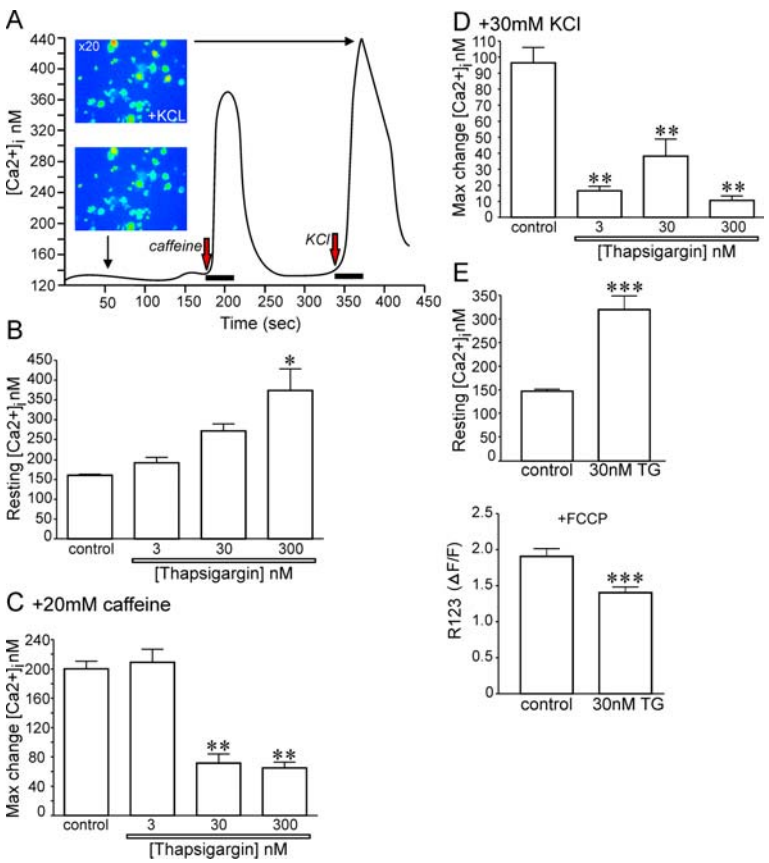

Figure 6 **Long-term treatment with TG to block SERCA activity generates a Ca^{2+} dysfunction phenotype that mimics the diabetic state**
(**A**) Typical Fura 2/AM fluorescence trace derived from a control untreated neuron. (**B**) Effect of 24 h treatment with increasing concentrations of TG on resting intracellular Ca^{2+} concentration. *$P<0.05$ versus control. (**C**) Impact of transient exposure (30 s) to 20 mM caffeine on control or neurons treated for 24 h with a range of TG doses. Presented is maximum (Max) change (increase) in intracellular Ca^{2+} concentration. **$P<0.01$ versus control and 3 nM TG. (**D**) Effect of transient (30 s) 30 mM KCl on intracellular Ca^{2+} concentration. **$P<0.01$ versus control. Values are means ± S.E.M. ($n=21–31$ neurons). (**E**) In a separate experiment, neurons were treated for 24 h with 30 nM TG and then loaded with Fura 2/AM and R123 and simultaneously imaged for intracellular Ca^{2+} and mitochondrial membrane potential. ***$P<0.01$ versus control. Values are means ± S.E.M. ($n=32–36$ neurons).

DISCUSSION

We have previously demonstrated that neurons derived from 3- to 5-month-old STZ-induced diabetic rats (an experimental model of Type 1 diabetes) undergo axonal dystrophy following 2–4 days in cell culture with evidence for distal loss of functional mitochondria, reduced plasticity and formation of axonal swellings (Zherebitskaya et al., 2009; Akude et al., 2010). This pathology is homologous with axonopathy seen in animal models and humans with diabetic neuropathy (Schmidt et al., 1997; Christianson et al., 2003; Quattrini et al., 2007). In the present study, analysis of Ca^{2+} homoeostasis in axons of neurons derived from diabetic rats and cultured for 1–2 days shows a decrease in resting ER Ca^{2+} content. Quantification of calnexin expression in axons, a marker of ER mass, revealed no major difference between control and diabetic cultures, indicating no changes in overall ER presence in the cells. Axonal expression of ER stress protein GRP78 also was not altered by a history of diabetes. Patch-clamp and pharmacological studies on cell bodies of sensory neurons showed that the function of SERCA pumps was depressed in diabetic cultures, as was expression of SERCA2a protein (confirmed in a previous *in vivo* study with intact lumbar DRG; Verkhratsky and Fernyhough, 2008), and could be responsible for impaired loading of Ca^{2+} into the ER. The results support previous work on acutely isolated neurons from diabetic rodents (Voitenko et al., 1999; Kostyuk et al., 2001; Huang et al., 2002; Kruglikov et al., 2004) and enforce the notion that early abnormalities in Ca^{2+} homoeostasis mediated by impaired SERCA functioning may trigger axonal degeneration seen in diabetes.

The $[Ca^{2+}]_{ER}$ imaging studies presented in Figure 5 reveal that Ca^{2+} uptake into the ER lumen was suppressed by at least 2-fold in diabetic cultures. Figure 6 shows that specific inhibition of SERCA activity using TG was able to closely mimic abnormalities in Ca^{2+} homoeostasis seen in diabetes, e.g. raised resting $[Ca^{2+}]_i$ and impaired ER Ca^{2+} release. The immunocytochemistry results in Figure 3 suggested a general loss of ER mass in axons in diabetic culture; however, this finding was not supported by the Western blotting approach using culture inserts (Figure 4). The Western blot data were generated relative to total protein and in diabetes a general down-regulation of protein occurs and so specific changes in calnexin may have been under-estimated. There is previous evidence of reduced expression of SERCA2a, and these data support the hypothesis that diabetes-induced SERCA deactivation underlies reduced Ca^{2+} loading in the ER. Diminished activity of SERCA could be solely due to loss of expression, and there is evidence that insulin can regulate SERCA activity in non-neuronal cells (Borge and Wolf, 2003; Abdallah et al., 2006). However, it is also feasible that impaired cellular bioenergetics may result in suboptimal ATP delivery for SERCA function since the respiratory chain activity and expression in DRG neurons is down-regulated in STZ-induced diabetic rats (Chowdhury et al., 2010; Akude et al., 2011). The cause of the latter feature of diabetes-induced impairment in neuronal function is complex and could also be the result of dysfunctional Ca^{2+} homoeostasis. Figure 6 demonstrates that TG-induced decrease in resting $[Ca^{2+}]_{ER}$ and a subsequent rise in resting $[Ca^{2+}]_i$, as seen in sensory neurons acutely isolated from diabetic rats and mice (Voitenko et al., 2000; Kostyuk et al., 2001; Huang et al., 2002; Kruglikov et al., 2004), was accompanied by mitochondrial inner membrane depolarization. Impaired Ca^{2+} homoeostasis leading to a rise in resting $[Ca^{2+}]_i$ may result in Ca^{2+} entry into the mitochondrion, primarily through the mitochondrial Ca^{2+} uniporter, raised intramitochondrial calcium concentration ($[Ca^{2+}]_m$) and mitochondrial membrane depolarization and altered bioenergetics (Verkhratsky and Toescu, 1998; Verkhratsky and Fernyhough, 2008).

Our observations show that ER membrane dysfunction in the form of aberrant SERCA activity was present, but in the absence of overt ER stress. The marker of ER stress, GRP78, did not undergo an elevation in expression in cell body or axons of cultured diabetic neurons. This confirmed preliminary work from our laboratory showing a lack of effect of diabetes on GRP78 expression in lumbar DRG or sciatic nerve of 2–3 month-old STZ-induced diabetic rats. While the loss of Ca^{2+} loading in the ER was not significant enough to trigger a measurable ER stress response in our system the possibility of induction of SOCE [SOC (store-operated calcium) entry] cannot be dismissed. Neurons have recently been demonstrated to exhibit SOCE and express the ER proteins STIM1 (stromal interaction molecule 1) and STIM2 that detect Ca^{2+} loading in the ER and link to SOC channel activity in the plasma membrane (Gruszczynska-Biegala et al., 2011). The permanent depletion of ER Ca^{2+} in diabetic neurons could be sensed by the STIM proteins and lead to an activation of SOCE and contribute to the rise in resting $[Ca^{2+}]_i$. In fact, in an HIV-induced model of sensory neuron degeneration blockade of SOCE was protective (Hoke et al., 2009).

The impact of a long-term rise in resting $[Ca^{2+}]_i$ on axonal function and association with axon degeneration has been discussed in detail elsewhere (Coleman, 2005; Stys, 2005; Verkhratsky and Fernyhough, 2008). Examples of Ca^{2+}-induced aberrant axon behaviour include fragmentation of microtubules due to activation of proteases of the proteasome or calpain and have been associated with the expression of the autophagy marker LC3 (Knoferle et al., 2010). In the optic nerve preparation, lesion-dependent LC3 expression has been linked to an initial axotomy-induced increase of $[Ca^{2+}]_i$ and to a secondary elevation in autophagy (Knoferle et al., 2010). This is of importance, since in lumbar DRG in STZ-induced diabetic rats there is preliminary evidence for markers of autophagy being enhanced (Towns et al., 2005). The Ca^{2+}-dependent activation of calpain in the axoplasm is also of particular interest, since this event has been directly linked to mitochondrial biology in axons and generation of axonal swellings (Kilinc et al., 2009). Other consequences of Ca^{2+} influx are of note: there is a general alteration in the phosphorylation balance, mediated for example by Ca^{2+}/CaM (calmodulin) binding to the phosphatase calcineurin or to CaM kinases

which signal to other kinases and thus may affect an array of proteins, including MAPs (microtubule-associated proteins) and motor proteins (Zempel et al., 2010). This array of Ca^{2+}-induced events could lead to cytoskeletal dissolution, mitochondrial dysfunction and eventually axonal degeneration.

In conclusion, axons of diabetic neurons exhibit impaired calcium homoeostasis with dysfunction primarily the result of sub-optimal SERCA activity and/or expression. The diminished ability of the ER to accumulate Ca^{2+} could lead to the rise in resting $[Ca^{2+}]_i$ observed in neurons from diabetic rats. The sub-optimal levels of Ca^{2+} within the ER lumen could also initiate SOCE that could contribute to a rise in resting $[Ca^{2+}]_i$. The two major consequences of the rise in resting $[Ca^{2+}]_i$ could be mitochondrial dysfunction, mediated though enhanced Ca^{2+} uptake and inner membrane depolarization, and a general effect of raised Ca^{2+} on an array of enzymes important for homoeostatic control of protein function in the axoplasm. The outcome is axonal degeneration through dissolution of the cytoarchitecture and/or loss of cellular bioenergetics.

ACKNOWLEDGEMENT

We thank Dr Gordon Glazner, University of Manitoba and St. Boniface Hospital Research Centre, for permitting access to the Carl Zeiss LSM510 confocal inverted microscope.

FUNDING

We thank St. Boniface Research for funding support. E.Z. and P.F. were supported by grants from CIHR (Canadian Institutes for Health Research) [grant number MOP-84214] and Juvenile Diabetes Research Foundation [grant number 1-2008-193]. E.A. and P.F. were supported by a grant from the National Science and Engineering Research Council [grant number 3311686-06] and subsequently a postgraduate scholarship from the Manitoba Health Research Council. J.S. was supported by a CIHR doctoral scholarship.

REFERENCES

Abdallah Y, Gkatzoflia A, Gligorievski D, Kasseckert S, Euler G, Schluter KD, Schafer M, Piper HM, Schafer C (2006) Insulin protects cardiomyocytes against reoxygenation-induced hypercontracture by a survival pathway targeting SR Ca^{2+} storage. Cardiovasc Res 70:346–353.

Akude E, Zherebitskaya E, Chowdhury SK, Smith DR, Dobrowsky RT, Fernyhough P (2011) Diminished superoxide generation is associated with respiratory chain dysfunction and changes in the mitochondrial proteome of sensory neurons from diabetic rats. Diabetes 60:288–297.

Akude E, Zherebitskaya E, Roy Chowdhury SK, Girling K, Fernyhough P (2010) 4-Hydroxy-2-nonenal induces mitochondrial dysfunction and aberrant axonal outgrowth in adult sensory neurons that mimics features of diabetic neuropathy. Neurotox Res 17:28–38.

Beiswenger KK, Calcutt NA, Mizisin AP (2008) Dissociation of thermal hypoalgesia and epidermal denervation in streptozotocin-diabetic mice. Neurosci Lett 442:267–272.

Borge PD Jr., Wolf BA (2003) Insulin receptor substrate 1 regulation of sarco-endoplasmic reticulum calcium ATPase 3 in insulin-secreting beta-cells. J Biol Chem 278:11359–11368.

Burdakov D, Petersen OH, Verkhratsky A (2005) Intraluminal calcium as a primary regulator of endoplasmic reticulum function. Cell Calcium 38:303–310.

Chowdhury SK, Zherebitskaya E, Smith DR, Akude E, Chattopadhyay S, Jolivalt CG, Calcutt NA, Fernyhough P (2010) Mitochondrial respiratory chain dysfunction in dorsal root ganglia of streptozotocin-induced diabetic rats and its correction by insulin treatment. Diabetes 59:1082–1091.

Christianson JA, Riekhof JT, Wright DE (2003) Restorative effects of neurotrophin treatment on diabetes-induced cutaneous axon loss in mice. Exp Neurol 179:188–199.

Christianson JA, Ryals JM, Johnson MS, Dobrowsky RT, Wright DE (2007) Neurotrophic modulation of myelinated cutaneous innervation and mechanical sensory loss in diabetic mice. Neuroscience 145:303–313.

Coleman M (2005) Axon degeneration mechanisms: commonality amid diversity. Nat Rev Neurosci 6:889–898.

Ebenezer GJ, O'Donnell R, Hauer P, Cimino NP, McArthur JC, Polydefkis M (2011) Impaired neurovascular repair in subjects with diabetes following experimental intracutaneous axotomy. Brain 134:1853–1863.

Fernyhough P, Gallagher A, Averill SA, Priestley JV, Hounsom L, Patel J, Tomlinson DR (1999) Aberrant neurofilament phosphorylation in sensory neurons of rats with diabetic neuropathy. Diabetes 48:881–889.

Fernyhough P, Huang TJ, Verkhratsky A (2003) Mechanism of mitochondrial dysfunction in diabetic sensory neuropathy. J Peripher Nerv Syst 8:227–235.

Francis G, Martinez J, Liu W, Nguyen T, Ayer A, Fine J, Zochodne D, Hanson LR, Frey WH II, Toth C (2009) Intranasal insulin ameliorates experimental diabetic neuropathy. Diabetes 58:934–945.

Glazner GW, Fernyhough P (2002) Neuronal survival in the balance: are endoplasmic reticulum membrane proteins the fulcrum? Cell Calcium 32:421–433.

Gruszczynska-Biegala J, Pomorski P, Wisniewska MB, Kuznicki J (2011) Differential roles for STIM1 and STIM2 in store-operated calcium entry in rat neurons. PLoS ONE 6:e19285.

Hall KE, Liu J, Sima AA, Wiley JW (2001) Impaired inhibitory G-protein function contributes to increased calcium currents in rats with diabetic neuropathy. J Neurophysiol 86:760–770.

Hall KE, Sima AA, Wiley JW (1995) Voltage-dependent calcium currents are enhanced in dorsal root ganglion neurones from the Bio Bred/Worchester diabetic rat. J Physiol 486 (Pt 2):313–322.

Hardingham GE, Arnold FJ, Bading H (2001) Nuclear calcium signaling controls CREB-mediated gene expression triggered by synaptic activity. Nat Neurosci 4:261–267.

Hoke A, Morris M, Haughey NJ (2009) GPI–1046 protects dorsal root ganglia from gp120-induced axonal injury by modulating store-operated calcium entry. J Peripher Nerv Syst 14:27–35.

Huang TJ, Price SA, Chilton L, Calcutt NA, Tomlinson DR, Verkhratsky A, Fernyhough P (2003) Insulin prevents depolarization of the mitochondrial inner membrane in sensory neurons of type 1 diabetic rats in the presence of sustained hyperglycemia. Diabetes 52:2129–2136.

Huang TJ, Sayers NM, Fernyhough P, Verkhratsky A (2002) Diabetes-induced alterations in calcium homeostasis in sensory neurones of streptozotocin-diabetic rats are restricted to lumbar ganglia and are prevented by neurotrophin-3. Diabetologia 45:560–570.

Huang TJ, Sayers NM, Verkhratsky A, Fernyhough P (2005a) Neurotrophin-3 prevents mitochondrial dysfunction in sensory neurons of streptozotocin-diabetic rats. Exp Neurol 194:279–283.

Huang TJ, Verkhratsky A, Fernyhough P (2005b) Insulin enhances mitochondrial inner membrane potential and increases ATP levels through phosphoinositide 3-kinase in adult sensory neurons. Mol Cell Neurosci 28:42–54.

Jolivalt CG, Lee CA, Ramos KM, Calcutt NA (2008) Allodynia and hyperalgesia in diabetic rats are mediated by GABA and depletion of spinal potassium-chloride co-transporters. Pain 140:48–57.

Kennedy WR, Wendelschafer-Crabb G, Johnson T (1996) Quantitation of epidermal nerves in diabetic neuropathy. Neurology 47:1042–1048.

Kilinc D, Gallo G, Barbee KA (2009) Mechanical membrane injury induces axonal beading through localized activation of calpain. Exp Neurol 219:553–561.

Knoferle J, Koch JC, Ostendorf T, Michel U, Planchamp V, Vutova P, Tonges L, Stadelmann C, Bruck W, Bahr M et al. (2010) Mechanisms of acute axonal degeneration in the optic nerve *in vivo*. Proc Natl Acad Sci USA 107:6064–6069.

Kostyuk E, Pronchuk N, Shmigol A (1995) Calcium signal prolongation in sensory neurones of mice with experimental diabetes. Neuroreport 6:1010–1012.

Kostyuk E, Voitenko N, Kruglikov I, Shmigol A, Shishkin V, Efimov A, Kostyuk P (2001) Diabetes-induced changes in calcium homeostasis and the effects of calcium channel blockers in rat and mice nociceptive neurons. Diabetologia 44:1302–1309.

Kruglikov I, Gryshchenko O, Shutov L, Kostyuk E, Kostyuk P, Voitenko N (2004) Diabetes-induced abnormalities in ER calcium mobilization in primary and secondary nociceptive neurons. Pflugers Arch 448:395–401.

Llano I, Gonzalez J, Caputo C, Lai FA, Blayney LM, Tan YP, Marty A (2000) Presynaptic calcium stores underlie large-amplitude miniature IPSCs and spontaneous calcium transients. Nat Neurosci 3:1256–1265.

Malik RA, Tesfaye S, Newrick PG, Walker D, Rajbhandari SM, Siddique I, Sharma AK, Boulton AJ, King RH, Thomas PK et al. (2005) Sural nerve pathology in diabetic patients with minimal but progressive neuropathy. Diabetologia 48:578–585.

Mattson MP, Gary DS, Chan SL, Duan W (2001) Perturbed endoplasmic reticulum function, synaptic apoptosis and the pathogenesis of Alzheimer's disease. Biochem Soc Symp 67:151–162.

Mizisin AP, Nelson RW, Sturges BK, Vernau KM, Lecouteur RA, Williams DC, Burgers ML, Shelton GD (2007) Comparable myelinated nerve pathology in feline and human diabetes mellitus. Acta Neuropathol 113:431–442.

Paschen W, Frandsen A (2001) Endoplasmic reticulum dysfunction – a common denominator for cell injury in acute and degenerative diseases of the brain? J Neurochem 79:719–725.

Patel S, Churchill GC, Galione A (2001) Coordination of Ca^{2+} signalling by NAADP. Trends Biochem Sci 26:482–489.

Patil C, Walter P (2001) Intracellular signaling from the endoplasmic reticulum to the nucleus: the unfolded protein response in yeast and mammals. Curr Opin Cell Biol 13:349–355.

Petersen OH, Tepikin A, Park MK (2001) The endoplasmic reticulum: one continuous or several separate Ca^{2+} stores? Trends Neurosci 24:271–276.

Quattrini C, Tavakoli M, Jeziorska M, Kallinikos P, Tesfaye S, Finnigan J, Marshall A, Boulton AJ, Efron N, Malik RA (2007) Surrogate markers of small fiber damage in human diabetic neuropathy. Diabetes 56:2148–2154.

Rose CR, Konnerth A (2001) Stores not just for storage. intracellular calcium release and synaptic plasticity. Neuron 31:519–522.

Schmidt RE, Dorsey D, Parvin CA, Beaudet LN, Plurad SB, Roth KA (1997) Dystrophic axonal swellings develop as a function of age and diabetes in human dorsal root ganglia. J Neuropathol Exp Neurol 56:1028–1043.

Sitsapesan R, McGarry SJ, Williams AJ (1995) Cyclic ADP-ribose, the ryanodine receptor and Ca^{2+} release. Trends Pharmacol Sci 16:386–391.

Solovyova N, Verkhratsky A (2002) Monitoring of free calcium in the neuronal endoplasmic reticulum: an overview of modern approaches. J Neurosci Methods 122:1–12.

Solovyova N, Veselovsky N, Toescu EC, Verkhratsky A (2002) Ca^{2+} dynamics in the lumen of the endoplasmic reticulum in sensory neurons: direct visualization of Ca^{2+}-induced Ca^{2+} release triggered by physiological Ca^{2+} entry. EMBO J 21:622–630.

Stys PK (2005) General mechanisms of axonal damage and its prevention. J Neurol Sci 233:3–13.

Sutko JL, Airey JA (1996) Ryanodine receptor Ca^{2+} release channels: does diversity in form equal diversity in function? Physiol Rev 76:1027–1071.

Thrower EC, Hagar RE, Ehrlich BE (2001) Regulation of Ins(1,4,5)P_3 receptor isoforms by endogenous modulators. Trends Pharmacol Sci 22:580–586.

Towns R, Kabeya Y, Yoshimori T, Guo C, Shangguan Y, Hong S, Kaplan M, Klionsky DJ, Wiley JW (2005) Sera from patients with type 2 diabetes and neuropathy induce autophagy and colocalization with mitochondria in SY5Y cells. Autophagy 1:163–170.

Verkhratsky A (2005) Physiology and pathophysiology of the calcium store in the endoplasmic reticulum of neurons. Physiol Rev 85:201–279.

Verkhratsky A, Fernyhough P (2008) Mitochondrial malfunction and Ca^{2+} dyshomeostasis drive neuronal pathology in diabetes. Cell Calcium 44: 112–122.

Verkhratsky A, Petersen OH (2002) The endoplasmic reticulum as an integrating signalling organelle: from neuronal signalling to neuronal death. Eur J Pharmacol 447:141–154.

Verkhratsky A, Toescu EC (1998) Calcium and neuronal ageing. Trends Neurosci 21:2–7.

Voitenko NV, Kostyuk EP, Kruglikov IA, Kostyuk PG (1999) Changes in calcium signalling in dorsal horn neurons in rats with streptozotocin-induced diabetes. Neuroscience 94:887–890.

Voitenko NV, Kruglikov IA, Kostyuk EP, Kostyuk PG (2000) Effect of streptozotocin-induced diabetes on the activity of calcium channels in rat dorsal horn neurons. Neuroscience 95:519–524.

Yagihashi S (1996) Pathology and pathogenetic mechanisms of diabetic neuropathy. Diabetes Metab Rev 11:193–225.

Zempel H, Thies E, Mandelkow E, Mandelkow EM (2010) Abeta oligomers cause localized Ca^{2+} elevation, missorting of endogenous Tau into dendrites, Tau phosphorylation, and destruction of microtubules and spines. J Neurosci 30:11938–11950.

Zheng JQ, Kelly TK, Chang B, Ryazantsev S, Rajasekaran AK, Martin KC, Twiss JL (2001) A functional role for intra-axonal protein synthesis during axonal regeneration from adult sensory neurons. J Neurosci 21:9291–9303.

Zherebitskaya E, Akude E, Smith DR, Fernyhough P (2009) Development of selective axonopathy in adult sensory neurons isolated from diabetic rats: role of glucose-induced oxidative stress. Diabetes 58:1356–1364.

Received 3 November 2011/9 December 2011; accepted 14 December 2011

Published as Immediate Publication 14 December 2011, doi 10.1042/AN20110038